JACS
JOURNAL OF THE AMERICAN CHEMICAL SOCIETY
Article
pubs.acs.org/JACS

Orientational Dynamics of Water at an Extended Hydrophobic Interface

Shunhao Xiao,[†] Florian Figge,[†] Guillaume Stirnemann,[‡] Damien Laage,[*,§] and John A. McGuire[*,†]

[†]Department of Physics and Astronomy, Michigan State University, East Lansing, Michigan 48824, United States

[‡]CNRS Laboratoire de Biochimie Théorique, Institut de Biologie Physico-Chimique, Univ. Paris Diderot, Sorbonne Paris Cité, PSL Research University, 13 rue Pierre et Marie Curie, 75005 Paris, France

[§]École Normale Supérieure-PSL Research University, Département de Chimie, Sorbonne Universités - UPMC Univ Paris 06, CNRS UMR 8640 PASTEUR, 24, rue Lhomond, 75005 Paris, France

ABSTRACT: We report on the orientational dynamics of water at an extended hydrophobic interface with an octadecylsilane self-assembled monolayer on fused silica. The interfacial dangling OH stretch mode is excited with a resonant pump, and its evolution followed in time by a surface-specific, vibrationally resonant, infrared-visible sum-frequency probe. High sensitivity pump−probe anisotropy measurements and isotopic dilution clearly reveal that the decay of the dangling OH stretch excitation is almost entirely due to a jump to a hydrogen-bonded configuration that occurs in 1.61 ± 0.10 ps. This is more than twice as fast as the jump time from one hydrogen-bonded configuration to another in bulk H_2O but about 50% slower than the reported out-of-plane reorientation at the air/water interface. In contrast, the intrinsic population lifetime of the dangling OH stretch in the absence of such jumps is found to be >10 ps. Molecular dynamics simulations of air/water and hexane/water interfaces reproduce the fast jump dynamics of interfacial dangling OH with calculated jump times of 1.4 and 1.7 ps for the air and hydrophobic interfaces, respectively. The simulations highlight that while the air/water and hydrophobic/water surfaces exhibit great structural similarities, a small stabilization of the OH groups by the hydrophobic interface produces the pronounced difference in the dynamics of dangling bonds.

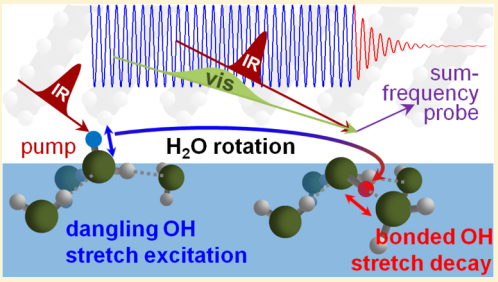

1. INTRODUCTION

Interfaces between aqueous solutions and extended hydrophobic surfaces play essential roles in numerous biological, chemical, and physical processes. Protein structural stability and conformational changes are driven in part by hydrophobic interactions and fluctuations of the hydration shell.[1,2] At oil−water phase boundaries, the rate constants for certain chemical reactions, such as Diels−Alder cycloadditions and Claisen rearrangements, are up to 5 orders of magnitude greater than the rate constants for the corresponding reactions in the neat liquid.[3] The acceleration of such "on-water" reactions is proposed to occur because of the availability of otherwise non-hydrogen-bonded OH, or dangling OH (dOH), groups at such surfaces for stabilizing the transition state by hydrogen bonding.[4] Fluctuations of hydrophobic adlayers may also play an important role in, e.g., electrochemistry.[5]

Despite the ubiquity of aqueous interfaces, experimental studies of the dynamics of water at extended interfaces began only recently. Most studies have focused on vibrational population relaxation of the hydrogen-bonded OH (bOH) stretch measured by a sum-frequency-generation probe following an infrared pump, referred to hereafter as pump−probe sum frequency generation or ppSFG.[6−8] The high frequency of the OH stretch modes means that in the liquid phase the excited states of these modes are negligibly populated. In this sense, the vibrational lifetime is irrelevant to processes such as structural rearrangements at thermodynamic equilibrium. Of more direct relevance to many interfacial processes are the orientational dynamics of water. Yet, the orientational motion of water at interfaces has been experimentally elusive[9,10] due to the difficulty of obtaining a high signal-to-noise ratio by ppSFG and the complicated manner in which orientational motion is reflected in SFG measurements.[11,12] Hence, computational studies have generally preceded experimental ones,[13,14] and to date there has been only a single pair of experimental measurements of orientational dynamics at the air/water interface.[9,10]

In contrast to the case of surfaces, the dynamics of bulk water have been extensively investigated by experiment as well as theory. In particular, water orientational dynamics are commonly characterized by the second-order Legendre polynomial time-correlation function $C_2(t)$, which is accessible to third-order time-resolved infrared spectroscopy. In the bulk at room temperature, $C_2(t)$ decays with a ∼2.5 ps time constant,[15,16] consistent with molecular dynamics (MD) simulations.[17,18] These dynamics are nondiffusive with large angular jumps between different hydrogen-bonded configurations mediated by a transition state consisting of a bifurcated

Received: December 19, 2014
Revised: February 18, 2016
Published: April 5, 2016

DOI: 10.1021/jacs.6b01820
J. Am. Chem. Soc. 2016, 138, 5551−5560

hydrogen bond (HB) that is part of a five-coordinate water molecule.[17,18] A key characteristic of these dynamics is the time between such jumps, which is 3.3 ps in bulk H_2O at room temperature.[18]

At a rigid hydrophobic interface, MD simulations have suggested that at room temperature the dOH groups are characterized by a 1.6 ps jump time to a tangential, hydrogen-bonded state.[14] The absence of hydrogen-bonding constraints on the dOH groups pointing toward the hydrophobic side of the interface contributes to the acceleration of the reorientation as compared to the bulk case. While this behavior is qualitatively similar at the air/water interface, simulation and experimental studies of the dOH reorientation at the latter interface found a significantly faster, ~1 ps time constant to jump from a dangling to a hydrogen-bonded state.[9,10,19] Until now, experimental evidence for a slowed jump at a hydrophobic interface has been missing.

Since dOH groups remain in a non-hydrogen-bonded state for <200 fs in neat bulk water,[20] the much-longer-lived dOH stretch found at a hydrophobic surface is a precise reporter of surface dynamics and is free of the ambiguities about the interfacial nature of the measured SFG response encountered in studies of the bOH modes in SFG.[8,21] Here we present ppSFG measurements of orientational and vibrational dynamics of the dOH group of pure H_2O and of an isotopic mixture of H_2O in D_2O at the interface with a self-assembled monolayer (SAM) of octadecylsilane (ODS) on fused silica. An essential element for resolving orientational dynamics from other dynamic processes is a high signal-to-noise ratio, but SFG signals are typically weak. We, therefore, perform ppSFG measurements in a total-internal-reflection geometry in which the Fresnel coefficients can lead to orders-of-magnitude enhancements in the SFG signal. Our experiments reveal that out-of-plane reorientation of the dOH to a bOH configuration is characterized by a 1.61 ± 0.10 ps time constant, about 50% slower than that reported for the air/water interface. We show that molecular dynamics (MD) simulations of the air/water and hydrophobic/water surfaces qualitatively reproduce these differences, with jump times of 1.4 and 1.7 ps, respectively, at the air/water and hydrophobic/water interfaces. We also discuss the structural similarities between the air/water and hydrophobic/water surfaces, which suggest that the slower dangling dynamics at the hydrophobic interface arises from an ~0.1 kcal/mol stabilization of these OH groups by the hydrophobic interface.

2. THEORETICAL FRAMEWORK FOR PROBING ORIENTATIONAL DYNAMICS

For probing dynamics at extended aqueous interfaces, ppSFG is the technique of choice as it offers surface, mode, and temporal sensitivity. However, a dipole-allowed SFG signal inherently requires an anisotropic molecular distribution, which complicates the analysis compared to the case of orientational anisotropy measurements in isotropic bulk liquids. The basic theory of static[22] and pump−probe[11,12,23] SFG has been described elsewhere. Considering only a vibrationally resonant infrared (IR) response and nonresonant visible (vis) and sum-frequency responses, the probe SFG intensity spectrum is given by $I(\omega_{\text{probeIR}}) \propto |\vec{P}^{(2)}(\omega_{\text{probeIR}})|^2$ where

$$\vec{P}^{(2)}(\omega_{\text{IRprobe}}) = \vec{\chi}^{(2)}(\omega_{\text{vis}}, \omega_{\text{probeIR}}) : \vec{E}(\omega_{\text{vis}})\,\vec{E}(\omega_{\text{probeIR}})$$

is the second-order probe polarization, $\vec{\chi}^{(2)}$ is the second-order nonlinear susceptibility, and $\vec{E}(\omega_i)$ is the electric field at frequency ω_i. To lowest order in the pump field and for a pump pulse that is short compared to the time scales for orientational and population dynamics, the second-order probe susceptibility at a time t after pump excitation becomes[12]

$$\begin{aligned}\chi^{(2)}_{\text{pr,ijk}}(\omega_{IR}, t) &= \langle(\hat{i}\cdot\vec{\alpha}(\vec{\Omega})\cdot\hat{j})(\vec{\mu}(\vec{\Omega}, \omega_{\text{IR}})\cdot\hat{k})\rangle_{\Omega} \\ &+ \langle(\hat{i}\cdot\vec{\alpha}(\vec{\Omega}_t)\cdot\hat{j})(\vec{\mu}(\vec{\Omega}_t)\cdot\hat{k})G(\vec{\Omega}_t, \vec{\Omega}_0)|\vec{\mu}(\vec{\Omega}_0)\cdot\hat{l}|^2\rangle_{\Omega_t,\Omega_0} \\ &\times |E_{\text{pu}}|^2 T_{\text{pu}}/\hbar^2 = \chi^{(2)}_{\text{no-pump},ijk}(\omega_{\text{IR}}) - R^{(4)}_{ijkll}(\omega_{\text{IR}}, t)|E_{\text{pu},l}|^2\end{aligned} \tag{1}$$

where $R_{ijkll}(\omega_{IR},t)$ is the fourth-order temporal response function described by the second pair of angled brackets, $\vec{E}_{\text{pu}}$ is the pump electric field and T_{pu} its temporal length, $\vec{\mu}(\omega_{\text{IR}})$ is the IR dipole derivative, $\vec{\alpha}$ is the Raman polarizability tensor, $\vec{\Omega}(t) = (\theta(t), \phi(t))$ represents the molecular orientation at time t, $G(\vec{\Omega}_t, \vec{\Omega}_0)$ is the Green's function describing the temporal evolution of the molecular orientation between times 0 and t, the angled brackets $\langle\rangle_{\Omega_i}$ represent averages over each Ω_i specified, and summation over repeated indices is assumed.

For orientational motion governed by diffusion, the Green's function in eq 1 can be expressed in terms of spherical harmonics and the rotational diffusion constant D_{or} as[24]

$$G(\Omega_t, \Omega_0) = \sum_{n=0}^{\infty}\sum_{m=-n}^{n} Y_n^m(\vec{\Omega}_t)Y_n^{m*}(\vec{\Omega}_0)\, e^{-n(n+1)D_{\text{or}}t} \tag{2}$$

The dOH orientational distribution at the water interface has $C_{\infty,v}$ symmetry, and its optical response is characterized by $\vec{\mu} = \mu_z\hat{z}$ and $\alpha_{ij} = \delta_{ij}\alpha_{ii}$, where $\alpha_{xx} = \alpha_{yy} = 0.32\ \alpha_{zz}$[25] and δ_{ij} is the Kronecker delta. In the absence of population relaxation and for free diffusion of the dOH within a cone of half angle θ_0 centered on the surface normal, the orientational correlation functions R_{zzzzz} and R_{zzzyy} can been shown to take the form:[12]

$$\begin{aligned}R_{zzzzz} &= A_{zz}(\theta_0) + B_{zz}(\theta_0)\, e^{-\nu_2^0(\nu_2^0+1)D_{\text{or}}t} \\ R_{zzzyy} &= A_{yy}(\theta_0) + B_{yy}(\theta_0)\, e^{-\nu_2^0(\nu_2^0+1)D_{\text{or}}t}\end{aligned} \tag{3}$$

where ν_n^m is a constant that depends on θ_0. (Even though the dOH group executes a large-amplitude jump when it forms a HB, its motion while dangling can be approximated by diffusion within a cone.[9]) The difference between $R_{zzzzz}(t)$ and a rescaled version of $R_{zzzyy}(t)$ directly yields a single-exponential decay governed by the rotational diffusion constant:

$$\begin{aligned}&R_{zzzzz}(t) - \frac{R_{zzzzz}(t \gg T_{\text{or}}^{-1})}{R_{zzzyy}(t \gg T_{\text{or}}^{-1})}R_{zzzyy}(t) \\ &= \left(B_{zz}(\theta_0) - \frac{A_{zz}(\theta_0)}{A_{yy}(\theta_0)}B_{yy}(\theta_0)\right)e^{-t/T_{\text{or}}}\end{aligned} \tag{4}$$

where $T_{\text{or}} = (\nu_2^0(\nu_2^0+1)D_{\text{or}})^{-1}$ and we drop the argument ω_{IR} in $R_{ijkll}(t)$ for brevity.

Experimentally, one can selectively probe the $\chi^{(2)}_{zzz}$ element of the nonlinear susceptibility of water by using a sufficiently large angle of incidence for the probe IR and visible light. In the case that other elements $\chi^{(2)}_{ijk}$ can be neglected and if we consider the normalized bleach of the SFG probe energy per laser pulse due

DOI: 10.1021/jacs.6b01820
J. Am. Chem. Soc. 2016, 138, 5551−5560

to, e.g., an *s*-polarized pump, we find a relative pump-induced bleach from eq 1 of

$$\beta_s(t) \equiv [U_{\mathrm{SFG,\,no\text{-}pump}} - U_{\mathrm{SFG,pu}}(t)]/U_{\mathrm{SFG,no\text{-}pump}} \propto R_{zzzyy}(t)$$

where we neglect terms of order $|E_{pu}|^4$. A *p*-polarized pump yields a similar result in terms of the response function $R_{zzzzz}(t)$. If the nonzero, long-delay bleach for *s*-polarized pump is scaled to match that for *p*-polarized pump, we directly obtain the orientational dynamics as in eq 4:

$$\Delta\beta(t) \equiv \beta_p(t) - \frac{\beta_p(t \gg T_{or})}{\beta_s(t \gg T_{or})}\beta_s(t) \propto e^{-k_{or}t} \tag{5}$$

where $k_{or} \equiv 1/T_{or}$. The preceding discussion neglected population relaxation, which when included yields

$$\Delta\beta(t) \propto e^{-k_{\Delta\beta}t} = e^{-(k_{or}+k_{dOH})t} \tag{6}$$

where $k_{dOH} = T_1^{-1}$ is the population relaxation rate.

One can also define a complementary term to $\Delta\beta(t)$, namely, the average

$$\bar{\beta}(t) \equiv \frac{1}{2}\left\{\beta_p(t) + \frac{\beta_p(t \gg T_{or})}{\beta_s(t \gg T_{or})}\beta_s(t)\right\} \propto A_{zz}(\theta_0)\, e^{-t/T_1} + \frac{1}{2}\left(B_{zz}(\theta_0) + \frac{A_{zz}(\theta_0)}{A_{yy}(\theta_0)}B_{yy}(\theta_0)\right) e^{-[k_{or}+T_1^{-1}]t} \tag{7}$$

B_{zz} and B_{yy} have opposite signs, so the amplitude of the second exponential will be reduced compared to the amplitude of the pure population term.

In general, orientational motion might not be diffusive, and the angular distribution of vibrationally excited and ground-state OH groups may depend on processes besides molecular reorientation, e.g., dipole−dipole coupling between groups. In the former case, the orientational dynamics might not follow a single-exponential decay. In the latter case, k_{or} might not directly reflect orientational motion of a molecular group. Nonetheless, $\Delta\beta(t)$ will still reveal the evolution of the orientational distribution of the difference between excited and ground state groups.

3. MATERIALS AND METHODS

Experimental Methods. We formed an octadecylsilane (ODS) SAM on an IR-grade fused silica isosceles trapezoidal prism with base angle of 60° following a variation on the method of Sagiv.[26] The prism was cleaned with a solution of NoChromix in sulfuric acid and deionized water; blown dry with N_2 gas; and then immersed in a solution of 0.1% octadecyltrichlorosilane (VWR, 97%) in *n*-hexadecane (Fisher Scientific, 99%), CCl_4 (Sigma-Aldrich, 99.5%), and $CHCl_3$ (DriSolv, 99%), all of which were anhydrous, in the volume ratios 80:12:8. Water contact angles on the SAM were 112° ± 4°. We mounted the prism on a Teflon cell, which was filled with deionized H_2O (Millipore, ≥18 MΩ) or an isotopic mixture of H_2O and D_2O (Sigma-Aldrich, 99.9%) in the molar ratio 1:2::H_2O:D_2O. The isotopic dilution was chosen as a compromise between, on the one hand, having a substantial majority of the dOH groups associated with HDO molecules and, on the other hand, a dramatic loss of signal associated with the N_{dOH}^2-dependence of the SFG intensity on the number density, N_{dOH}, of dOH groups at the interface.

The dOH stretch mode was excited with broadband (~45 cm^{-1} full-width at half-maximum) IR and narrowband 800 nm light. We generated the IR in a $KTiOPO_4$ crystal by mixing ~100 fs pulses of light at a wavelength of 1.13 μm with ~0.5 mJ of 100 fs, 800 nm pulses from a 1 kHz Ti:sapphire laser amplifier (SpectraPhysics Spitfire PRO-XP). The 1.13 μm light was generated by doubling the idler from a β-BaB_2O_4-based optical parametric amplifier pumped by 1 mJ of the Ti:sapphire laser output. To minimize the effects of atmospheric water vapor on the IR pulses, the DFG crystal and the IR beam path from the DFG crystal to the sample were maintained within an enclosure purged with dry N_2 gas. Only the final ~125 mm of the IR beam path was in atmosphere. The 800 nm pulses for SFG were spectrally narrowed to ~0.5 nm (8 cm^{-1}) in a pulse shaper consisting of a f = 0.5 m focal-length spherical mirror and a 1200 grooves/mm grating. The narrowband 800 nm pulse yields a one-to-one correspondence between the SFG and IR spectra: $\omega_{IR} = \omega_{SFG} - \omega_{800\ nm}$. Typical IR pump, IR probe, and 800 nm energies were 1.7, 1.7, and 5 μJ per pulse, respectively. A f = 75 mm (f = 400 mm) focal length lens produced IR (visible) focal spot diameters of 300 μm (250 μm) based on measurement of the power transmitted by a 250 μm diameter pinhole and assuming circular Gaussian spatial modes. The SFG data presented here were detected in *upp* configuration (SFG output unanalyzed and 800 nm and probe IR input *p*-polarized), but separate measurements confirmed that the probe SFG was *p*-polarized. A $CdGa_2S_4$ half-wave plate (UAB Altechna) was used to rotate the pump polarization between *p* and *s*. External to the prism and relative to the water interface normal, $\theta_{IR}^{probe} = \theta_{IR}^{pump} + 17.8°$ and $\theta_{800} = \theta_{IR}^{pump} + 24.5°$. The external angle of incidence of the IR pump beam relative to the fused-silica/ODS surface normal was $\theta_{IR,ext}^{pump} = 52.0°$ so that the probe SFG was generated in a total-internal-reflection geometry. The incident angles and Fresnel factors at the ODS/water interface result in the $\chi^{(2)}_{zzz}$ component of the nonlinear susceptibility accounting for >90% of the probe SFG signal and pump-induced bleach.

The SFG signal was detected with a liquid-N_2-cooled CCD camera (Princeton Instruments Spec-10:400B/LN) mounted on a 0.3 m imaging spectrometer (Acton Instruments SP2300) with a 1200 lines/mm grating. The SFG beam was focused to a width of ~0.05 mm at the spectrometer entrance. Combined with the 800 nm bandwidth, this yields a resolution of ~9 cm^{-1}. As described by Ghosh et al.,[27] we used a galvanometer-mounted mirror to separate pumped and unpumped probe SFG pulses on the CCD.

Theoretical Methods. We have performed molecular dynamics simulations of an air/water interface and of a typical hydrophobic/water interface that is distinct from the system used in the experiments but more readily modeled. To have a meaningful and rigorous comparison of the water dynamics in these two simulated systems, we have propagated the two trajectories under the same conditions and with the same water force field. An essential aspect of the subsequent analysis of these trajectories is the proper identification of interfacial dangling OH groups. We use here the instantaneous interface,[28] which is a significant improvement over prior works[19] that considered the average Gibbs interface and therefore ignored the ripples at the interface and incorrectly included transient dangling OH groups from the bulk in the interfacial population.

Simulation Details. In our simulations, we approximate the ODS SAM/water interface with the interface between water and a hexane phase. The simulation box contains water molecules for $z > 0$ and hexane molecules for $z < 0$ and was created by combining two 4 nm cubic boxes containing, respectively, 295 hexane molecules and 2135 water molecules inserted randomly. After minimization, the box was equilibrated in the NPT ensemble with Langevin dynamics for 2 ns. Finally, the system was propagated in the microcanonical ensemble for 1 ns, and the resulting data was used for the analysis. For the water vapor/liquid interface simulation, we used a previously equilibrated 4 nm cubic box under ambient conditions. We then increased the box size in the z direction to 10 nm and propagated the system in the microcanonical ensemble for 2 ns. After another short equilibration under these new conditions, a production run was propagated for 1 ns. For both systems, the average temperature in the production runs was 300 ± 1 K. We used the center-of-mass motion removal option of NAMD to avoid oscillations of the liquid water in the simulation box. All molecular dynamics (MD) simulations were performed using the NAMD2[29] software, the SPC/E water model,[30] and the CHARMM force field for hexane.[31] Ewald summation was employed to describe long-range electrostatic interactions, and periodic boundary conditions

DOI: 10.1021/jacs.6b01820
J. Am. Chem. Soc. 2016, 138, 5551−5560

were applied. Water reorientation dynamics in the bulk region of both systems (defined as the outermost region with respect to the surface) are very similar, with calculated jump times of 3.1−3.2 ps, in agreement with bulk jump times under similar conditions.[18]

Definition of HB States and the Instantaneous Interface. We define the instantaneous interface using the approach of Willard and Chandler.[28] A three-dimensional grid with a bin size of 1 Å is constructed, and the water density in each grid element is evaluated at each time step. The instantaneous interface is then defined as an iso-density surface (close to one-half of the bulk density[28]) in this grid. The average height of each point of the surface over the entire duration of the simulation defines the Gibbs surface. At each simulation time step, dangling and tangential OH groups are defined based on geometric criteria on their position and their orientation with respect to the instantaneous interface. Dangling groups should be located at less than 2 Å from the interface and their angle with respect to the normal vector at the closest point on the interface should not exceed 30° (Figures 5a and 6e, f). Tangential groups are defined using the same distance criterion, but their angle to the surface normal vector is defined to lie in the range 60°−120° (Figure 6e, f).

Calculation of Jump Times. For each OH group, we calculate the water HB exchange time, or jump time, as the average time to switch from a stable HB with a given acceptor to another stable HB with a different acceptor.[18] When the OH is in such a state that a HB cannot be defined (i.e., in a dangling state), the jump time is calculated as the average time to form a stable HB with a water partner starting from a dangling state, and vice versa.[14] The jump time is calculated as the integral of the cross-correlation function between the initial (I) and final (F) states, which are defined within the stable states picture (this does not apply for the dangling state) and using absorbing boundary conditions in the final state.[18] More details about this approach and its application to the study of water dynamics can be found elsewhere.[18,32]

Electric Field Distributions. We also calculate the electric field experienced by each water OH group. We calculate the projection on each OH axis of the electric field at the corresponding H atom resulting from all intermolecular interactions within a distance equal to half of the smallest simulation box side. This electric field is an indication of the strength of the HBs accepted by the water OH group, and it can also be related to experimental observables such as the OH stretch frequency.[33,34]

4. RESULTS

Figure 1 shows a SFG spectrum of the dOH stretch at the ODS/H_2O interface. The dOH peak is at 3680 cm^{-1}, in agreement with previous reports.[35,36] The input IR spectrum of our degenerate pump and probe is seen in the SFG spectrum from a silver surface and is less than twice the width of our dOH spectrum so that the initial excitation of the bOH stretch is negligible.

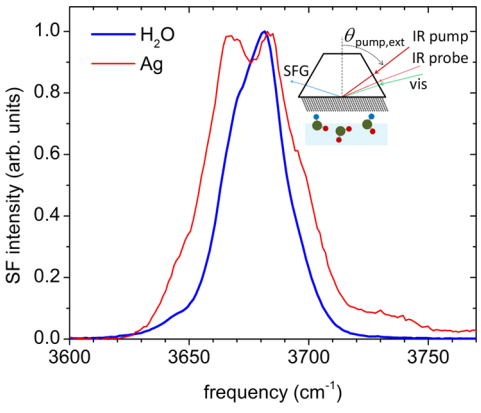

Figure 1. SFG probe spectrum of the dangling OH stretch from the octadecylsilane/H_2O interface (blue curve) and from a silver surface (red curve) for which the instantaneous response indicates the IR excitation spectrum. Inset is an illustration of the optical geometry.

Figure 2 shows the normalized SFG probe intensity dynamics ($U_{norm} \equiv U(t)/U(t<-1.2\ ps)$) for the dOH stretch at the ODS/H_2O (a) and ODS/H_2O:D_2O (b) interfaces. Throughout this paper, we only fit data at delays $t \geq 0.6$ ps, by which time the pump pulse has almost completely passed. To focus on the pump-induced dynamics, we consider the bleach $\beta(t) \equiv 1 - U_{norm}(t)$. For $t \geq 0.6$ ps, U_{norm} and the equivalent bleach are well described by a global biexponential fit using a common slow time constant of 15 ± 2 ps. The second, fast time constant for pure H_2O at $t \geq 0.6$ ps is 1.34 ± 0.03 ps for *p*-pump and 1.55 ± 0.04 ps for *s*-pump. (Error bars in graphs represent the standard deviation of the measurement. All other uncertainties in this report are the standard error.) The 1.34 ± 0.03 ps time constant agrees with earlier measurements[6] but is much slower than the 0.84 ps monoexponential decay reported for dOH at the air/H_2O surface.[10] In the isotopically diluted case, equivalent fits yield fast time constants of 1.13 ± 0.04 and 1.38 ± 0.08 for *p*- and *s*-pump, respectively. We observe that β_p and β_s at long delays are linearly proportional to the pump pulse energy. At the ODS/water interface, the higher-energy portion of the bOH stretch spectrum is associated with an IR dipole moment opposite that of the dOH stretch, which yields a contribution to $\chi^{(2)}$ of opposite sign[36] to the contribution from the dOH stretch. The incomplete recovery on a 50 ps time scale is likely due to a slight, transient rise in temperature that weakens the HB network in the immediate vicinity of the interface, resulting in a blueshift of the bonded OH spectrum.[6,7,37] We can then plot in Figure 2 the *scaled s*-pump response: $U_{s,scaled}(t) = 1 - [\langle\beta_p(t > 15\ ps)\rangle/\langle\beta_s(t > 15\ ps)\rangle]\beta_s(t)$. Overlap of the scaled *s*-pump signal with the *p*-pump data indicates that at long delays the *p*- and *s*-pump dynamics are identical, while the difference at early delays reflects the pump-induced anisotropy in the dOH excited and ground state populations.

Some samples exhibit SFG spectra with a small second feature peaked 10−20 cm^{-1} to the blue of the primary dOH peak. These spectra coincide with ppSFG traces showing weak but clear quantum beats with a frequency of ∼20 cm^{-1} and decaying with a time constant of ∼1 ps. These features likely arise from dOH groups associated with H_2O or HDO molecules trapped between the ODS SAM and fused silica.[38,39] The present study focuses on samples where we see no signatures of such secondary dOH populations within our experimental sensitivity.

5. ANALYSIS AND DISCUSSION

In Figure 3, we highlight the dynamics by plotting the difference $\Delta\beta(t) = \beta_p(t) - \beta_{s,scaled}(t)$, as defined in eq 5, as well as the average bleach minus its long-delay value:

$$\bar{\beta}'(t) = \bar{\beta}(t) - \bar{\beta}(t > 25ps)$$

where $\bar{\beta}(t) \equiv \frac{1}{2}\left[\beta_p(t) + \frac{\langle\beta_p(t > 25ps)\rangle}{\langle\beta_s(t > 25ps)\rangle}\beta_s(t)\right]$, as defined in eq 7. For $t \geq 0.6$ ps, a single-exponential fit of $\Delta\beta(t)$ for H_2O yields a time constant of $k_{\Delta\beta}^{-1}$ = 0.74 ± 0.05 ps. In contrast, biexponential fits to $\bar{\beta}'(t)$ starting at 0.6 and 2.0 ps yield fast time constants of 1.42 ± 0.02 and 1.46 ± 0.06 ps, respectively. As noted in discussing eq 7, at early times, the evolution of $\bar{\beta}(t)$ depends on both orientational and population dynamics,

DOI: 10.1021/jacs.6b01820
J. Am. Chem. Soc. 2016, 138, 5551−5560

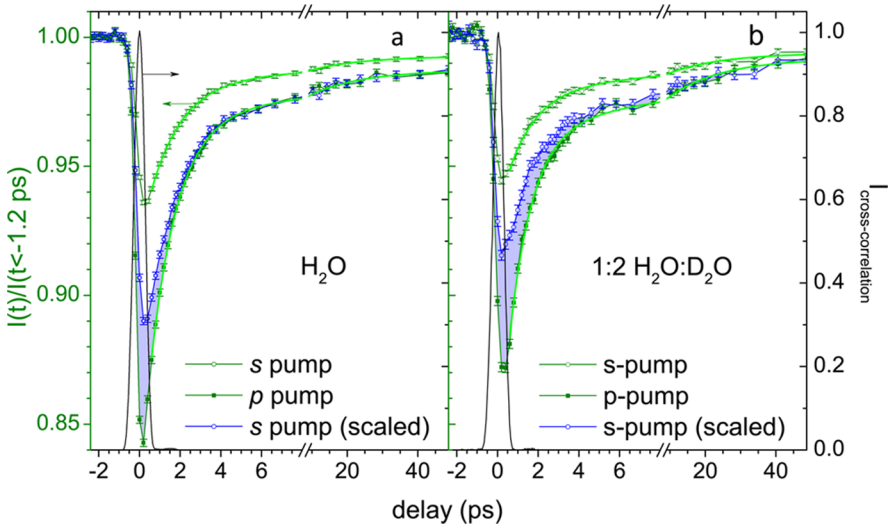

Figure 2. Time-resolved sum-frequency signal for the dOH stretch at the ODS/water interface normalized to the SFG signal at $t < -1.2$ ps for (a) pure H_2O and (b) H_2O:D_2O (1:2 molar ratio). The difference between the scaled *s*-pump and the *p*-pump data is highlighted by blue shading. The black curve is the third-order cross-correlation at $\omega_3 = \omega_{800} + 2\omega_{IR}$ from the fused silica prism taken in the exact same configuration as the ppSFG measurements; this establishes time $t = 0$ and indicates the instrument temporal resolution. Biexponential fits to I_{norm} at $t \geq 0.6$ ps are shown by the thick green curves.

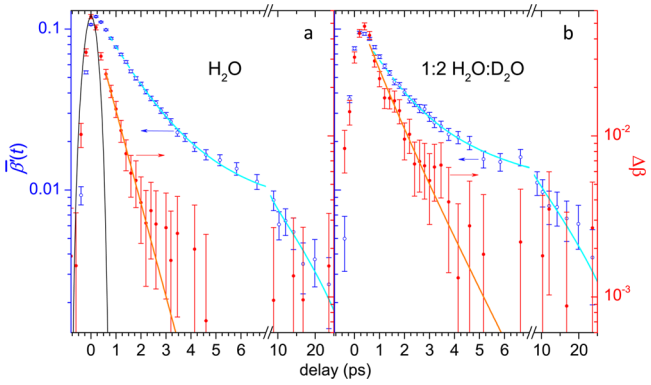

Figure 3. dOH stretch SFG dynamics at the (a) ODS/H_2O and (b) ODS/H_2O:D_2O interfaces showing the decay of the average bleach $\bar{\beta}'$ (open blue circles) relative to the long-delay bleach and the difference $\Delta\beta(t)$ (solid red circles) between the *p*-pump and scaled *s*-pump data. Solid curves show biexponential fits (cyan) for $t \geq 2.0$ ps and single-exponential fits (orange) for $t \geq 0.6$ ps. The dashed cyan curves illustrate the extension of the biexponential fit curves to the range [0.6, 2.0 ps]. Shown by the solid black curve in (a) is the third-order cross correlation.

though the former are suppressed compared to in the case of $\Delta\beta(t)$. The consistency of the fast time constant for $\bar{\beta}(t)$ obtained for fits starting at 0.6 and 2.0 ps indicates that the anisotropy underlying $\Delta\beta(t)$ contributes negligibly to $\bar{\beta}'(t)$ for H_2O. Nonetheless, to more confidently rule out contributions of pure orientational dynamics to measurements of population relaxation, we use the fit of $\bar{\beta}'$ at $t \geq 2.0$ ps to arrive at the population decay rate of the dOH stretch of $k_{dOH} = (1.46 \pm 0.06\ \text{ps})^{-1}$. Following eq 6, we subtract this rate from the decay rate of $\Delta\beta(t)$ to obtain a rate constant for the relaxation of the pump-induced orientational anisotropy in the difference between excited and ground state populations of the dOH stretch of $k_{or} = k_{\Delta\beta} - k_{dOH} = (1.50 \pm 0.10\ \text{ps})^{-1}$.

We observe that, within experimental uncertainty, $k_{or} = k_{dOH}$. This is understood as follows. Since we probe $\chi^{(2)}_{zzz}$, the orientational motions to which we are sensitive are those involving changes in the polar angle θ relative to the surface normal. Such motion leads to a decay in the pump-induced anisotropy at rate k_{or}. However, such motion also leads to a reconfiguration of a dOH to a bOH, which moves the stretch frequency out of the dOH stretch spectral window and thus appears as a population relaxation mechanism contributing to k_{dOH}.

As discussed in detail below, in principle k_{or} might be determined by more than the jump rate from a dOH to a bOH configuration. For example, through-space dipole−dipole couplings can alter the angular distribution of excited and ground-state dOH stretch populations without causing a change of the orientation of the dOH groups that are involved. If such nonrotational mechanisms contribute significantly to the measured ppSFG data in neat H_2O, this will be revealed by *slower* ppSFG dynamics in isotopically diluted water. To fit $\bar{\beta}'(t)$ and $\Delta\beta(t)$ for the isotopic mixture, we note that for a 1:2 dilution, 1/3 of dOH are associated with H_2O molecules, while 2/3 are associated with HDO molecules. As a first approximation, we assume that intermolecular dynamics remain unchanged for the H_2O molecules. We then require that 1/3 of the ppSFG signal decay follows the fit for pure H_2O and fit the ppSFG data with a 2/3 weighting of a second population corresponding to the HDO molecules. The assumption of identical intermolecular dynamics for H_2O populations in isotopically diluted and pure water means that any actual slowing of dynamics for H_2O in isotopically diluted water will be ascribed to the HDO population when fitting. The real dynamics of the HDO population should then be *faster* than our fit reveals. Fitting $\bar{\beta}'(t)$ for H_2O:D_2O with a second fast exponential decay associated with the HDO molecules yields a rate constant for the HDO dOH population of $k_{dOH}^{HDO} = (1.41 \pm 0.21\ \text{ps})^{-1}$. This is statistically indistinguishable from k_{dOH} measured for pure H_2O. Notably, the fitted value of k_{dOH}^{HDO} encompasses a range of rates equal to or *greater* than what is found for pure H_2O. This indicates that the population

DOI: 10.1021/jacs.6b01820
J. Am. Chem. Soc. 2016, 138, 5551−5560

dynamics of the dOH are not significantly affected by isotopic dilution.

Assuming that orientational motion is identical for H_2O and HDO molecules, we fit $\Delta\beta(t)$ for H_2O:D_2O with a single exponential decay. For $t \geq 0.6$ ps, we obtain a rate constant of $k_{\Delta\beta} = (1.02 \pm 0.08\ \text{ps})^{-1}$. Naively, this suggests that in the isotopic mixture $k_{or} = k_{\Delta\beta} - k_{dOH} = (3.7 \pm 1.8\ \text{ps})^{-1}$, which is at odds with k_{or} determined from pure H_2O. We attribute the decrease of $k_{\Delta\beta}$ obtained for the isotopic mixture compared to $k_{\Delta\beta}$ obtained for pure H_2O to the reduced signal-to-noise ratio inherent in isotopic dilution, which results in our scaling of the *s*-pump data being less accurate than for pure H_2O, and also to the fact that $\Delta\beta$ is determined from a difference in data traces and so is more susceptible to such inaccuracies than is the average $\bar{\beta}$. Further support and quantitative refinement of our interpretation of the ppSFG data can be found by considering the detailed mechanisms of population and orientational relaxation of the dOH stretch.

Decay Mechanisms of the Dangling OH Stretch. The processes contributing to the population and orientational dynamics of the dOH stretch and the consequent evolution of the ppSFG signal are illustrated in Figure 4. The superscripts *d*, *b*, *F*, and *B* indicate respectively dOH, bOH, "forward" transfer of energy from a dOH stretch to a bOH stretch mode, and "backward" transfer from a bOH stretch to a dOH stretch mode. The processes include

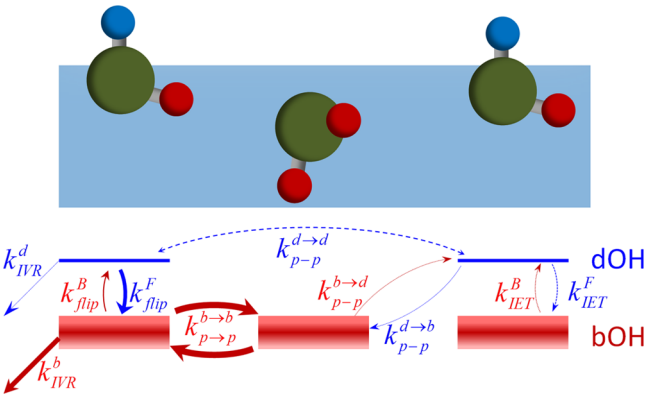

Figure 4. Rate constants for couplings between and decay of OH stretch modes of water at a hydrophobic interface. The thickness of the arrows corresponds qualitatively to the relative magnitudes of the corresponding rate constants.

(1) a forward jump of the dOH to a bOH configuration with rate k^{F}_{jump};[10]
(2) intramolecular energy transfer (IET) to the bOH stretch of the same H_2O molecule with rate k^{F}_{IET};[40]
(3) irreversible intramolecular vibrational relaxation (IVR) of the dOH stretch excitation to, e.g., the overtone of the molecule's bending mode, with rate k^{d}_{IVR};[41]
(4) dipole−dipole coupling to bOH (dOH) on other H_2O molecules with rate k^{F}_{p-p} ($k^{d\to d}_{p-p}$).[42]

The dynamics of the bOH stretch modes are governed by equivalent processes: (1) the backward jump of a bOH to a dOH with rate k^{B}_{jump}; (2) IET to dOH with rate k^{B}_{IET}; (3) IVR with rate k^{b}_{IVR}; and (4) dipole−dipole coupling to a dOH on a different H_2O molecule or to another bOH with respective rates k^{B}_{p-p} and $k^{b\to b}_{p-p}$. Only the jump processes directly involve orientational *motion* of a dOH, but all reversible processes (i.e., all processes but IVR) can contribute to the evolution of the orientational distribution of the population difference between ground- and excited-state dOH stretch groups. To determine k^{F}_{jump} and k^{B}_{jump}, we must account for the time scales of the various processes in Figure 4.

We list the rates of Figure 4 in Table 1. We exclude k^{F}_{jump}, which is to be determined, and k^{F}_{p-p}, k^{B}_{p-p}, and $k^{d\to d}_{p-p}$, which are expected to be very slow due to the r^{-6} distance-dependence of dipole−dipole coupling[42] and non-Condon effects that reduce the dOH stretch dipole transition matrix element by a factor of 3 relative to that of bOH.[46,47] The essential conclusion is that k^{b}_{IVR} and $k^{b\to b}_{p-p}$ dominate all other rates.

Table 1. Rate Constants of the Dominant Processes Shown in Figure 4

	H_2O		H_2O:D_2O::1:2	
term	value	source	value	source
k^{b}_{IVR}	$(0.2\ \text{ps})^{-1}$	refs 6, 7, 43	$(1.5\ \text{ps})^{-1}$	ref 44
$k^{b\to b}_{p-p}$	$\geq(0.15\ \text{ps})^{-1}$	ref 43	$\geq(1.6\ \text{ps})^{-1}$	ref 42
k^{F}_{IET}	$(13\ \text{ps})^{-1}$	refs 44, 45 and text	$\ll(13\ \text{ps})^{-1}$	same
R_{IET}	0.37	ref 10	0.0025	same
R	1/11	ref 14 and text	same	same

Determination of the Forward Jump Rate. Because of the dramatic difference between rate constants, k^{F}_{jump} can be directly determined from the experimental data. We define a rate of irreversible relaxation of the bOH stretch by $k^{b}_{irr} = k^{b}_{IVR} + k^{b\to b}_{p-p}$. Dipole−dipole coupling does not directly produce population relaxation. In our experiment only the dOH stretch is optically excited, so bOH groups are excited only by energy transfer from or reorientation of an excited dOH. Dipole−dipole couplings lead to transfer of bOH stretch excitations to bOH groups further from the initially excited dOH and the interface. Given that for pure H_2O k^{b}_{IVR}, $k^{b\to b}_{p-p} \gg k^{F}_{IET}$, k_{or}, the excited OH stretch population flows away from the interfacial dOH groups, and any transfer of excitation from a dOH to a bOH represents effectively irreversible population relaxation. This means that

$$k_{\bar{\beta}} \equiv k_{dOH} = k^{F}_{jump} + k^{F}_{IET} \tag{8}$$

In addition to leading to population decay of the excited dOH stretch, forward jumps change the orientational distribution of the excited dOH stretch such that

$$k_{\Delta\beta} = k^{F}_{jump} + k_{dOH} = 2k^{F}_{jump} + k^{F}_{IET} \tag{9}$$

The difference between $k_{\bar{\beta}}$ and $k_{\Delta\beta}$ provides an experimental constraint on k^{F}_{IET}:

$$k^{F}_{IET} = 2k_{\bar{\beta}} - k_{\Delta\beta}$$

For $k_{\bar{\beta}} = (1.46 \pm 0.06\ \text{ps})^{-1}$ and $k_{\Delta\beta} = (0.74 \pm 0.05\ \text{ps})^{-1}$, we find $k^{F}_{IET} = 0.019 \pm 0.107\ \text{ps}^{-1}$, which implies that $1/k^{F}_{IET} \geq 8$ ps, consistent with the value of 13 ps determined below and given in Table 1. For $1/k^{F}_{IET} = 13$ ps and the experimental value of $k_{\bar{\beta}}$, we find from eq 8 that $k^{F}_{jump} = (1.64 \pm 0.08\ \text{ps})^{-1}$. Similarly, from eq 9, we find $k^{F}_{jump} = (1.57 \pm 0.11\ \text{ps})^{-1}$. If we take for the uncertainty in k^{F}_{IET} the difference between the upper limit from experiment and the estimated value in Table 1 so that $k^{F}_{IET} = (13 \pm 8.4\ \text{ps})^{-1}$, the uncertainties on $1/k^{F}_{jump}$ from eqs 8 and 9 become 0.15 and 0.13 ps, respectively. Averaging these results, we obtain $k^{F}_{jump} = (1.61 \pm 0.10\ \text{ps})^{-1}$. The

DOI: 10.1021/jacs.6b01820
J. Am. Chem. Soc. 2016, 138, 5551−5560

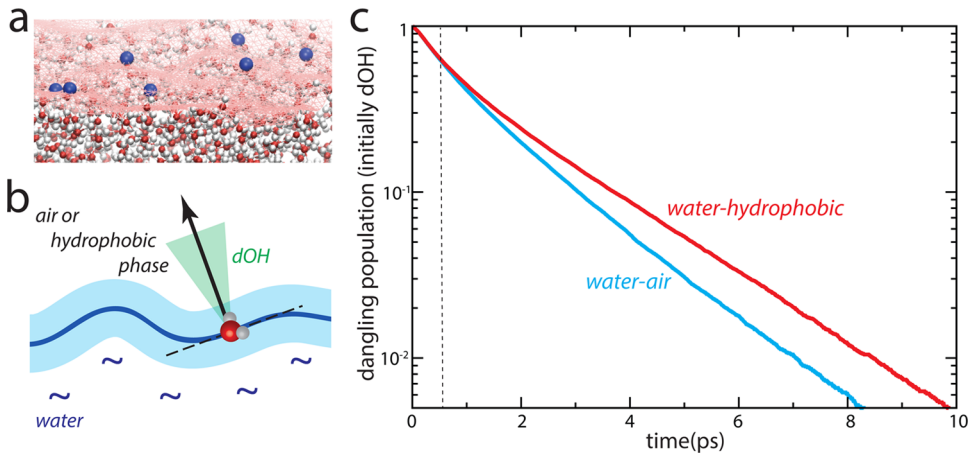

Figure 5. Identification and characterization of dangling OHs at extended interfaces. (a) MD snapshot of the air/liquid interface. Once the instantaneous interface has been determined (red mesh), geometric criteria (b) are used to define dangling OHs (blue spheres). The HB jump time-correlation functions[18] (c) are shown for the two interfaces (blue, air/water; red, hydrophobic/water). They correspond to the population of initially dangling interfacial OHs until they form a stable HB with a water partner.

conclusions of the preceding analysis are confirmed by detailed modeling.

Rate Equation Model of OH Stretch Population Dynamics. A more thorough accounting of the influence of various factors on the ppSFG dynamics can be made through a rate equation model of the dOH population and the bOH population directly coupled to the dOH population, i.e., the population of excited bOH associated with either a molecule with a dOH or a molecule that can jump to a dOH configuration. Ignoring dipole−dipole interactions other than those between two bOH groups, the dynamics illustrated in Figure 4 are expressed as

$$\dot{N}_{d1} = -(k^{F} + k^{d}_{IVR})N_{d1} + k^{B}N_{b1}$$
$$\dot{N}_{b1} = k^{F}N_{d1} - (k^{B} + k^{b}_{irr})N_{b1} \quad (10)$$

where $k^{F} \equiv k^{F}_{jump} + k^{F}_{IET}$, $k^{B} \equiv k^{B}_{jump} + k^{B}_{IET} = Rk^{F}_{jump} + R^{B}_{IET}k^{F}_{IET}$, and as above, $k^{b}_{irr} = k^{b}_{IVR} + k^{b\to b}_{p-p}$.

For the parameters in Table 1, a 1.46 ps time constant for the decay of $\bar{\beta}$ is best reproduced in eq 10 by $k^{F}_{jump} = (1.62\ \text{ps})^{-1}$. The rate equation model can be modified to capture the full dynamics observed for $k_{\bar{\beta}}$, including the slow time constant, by adding the contribution of a third population, that of ground state bOH stretches with a blue-shifted transition frequency after dissipation of the initial stretch excitation. The results are the same as found from eq 8 insofar as a forward jump time of 1.64 ps still yields the best fit to the data given the parameters of Table 1. Within the uncertainty in the data, analysis of the data for isotopically diluted water using the corresponding values of the rate constants from Table 1 yields values of k^{F}_{jump} consistent with the value of $k^{F}_{jump} = (1.61 \pm 0.10\ \text{ps})^{-1}$ determined from pure H_2O.

Equation 10 allows us to test the impact of variations in the rate constants from the values given in Table 1. It has been reported (without mechanistic explanation) that k^{b}_{IVR} could be as slow as $(0.8\ \text{ps})^{-1}$ at the molecular layers nearest a *bare* fused silica interface. However, even if that were the case for an ODS-coated surface, it would only imply a forward jump time 0.1 ps faster than determined above. Otherwise, the only parameter from Table 1 that is not firmly grounded in experimental measurements is $R \equiv k^{B}_{jump}/k^{F}_{jump}$. In particular, Hsieh et al. argue that for the air/water interface R = 1/1.7, which is 6.5 and 7.5 times larger than the values determined by simulations here and in ref.[14] For fast k^{b}_{irr}, though, the modeled dynamics are relatively insensitive to the exact value of *R*. In particular, for R = 1/1.7, a fast rate constant of $(1.46\ \text{ps})^{-1}$ for $k_{\bar{\beta}}$ is reproduced in our rate equation model by a forward jump time of 1.58 ps.

The largest sources of uncertainty in our reported value of k^{F}_{jump} are the experimental data and the uncertainty in k^{F}_{IET}. Therefore, it is worth considering estimates on the value of the latter. Above, we noted that the experimental data for pure H_2O place an upper limit of $k^{F}_{IET} \lesssim (8\ \text{ps})^{-1}$. From the difference in k_{dOH} measured for pure H_2O and for HDO, we also conclude that $k^{F,H_2O}_{IET} \approx k^{d,H_2O}_{dOH} - k^{d,HDO}_{dOH} < (10\ \text{ps})^{-1}$. These experimental limits on k^{F,H_2O}_{IET} are consistent with an estimate by perturbation theory. The vibrational wave function of the excited dOH stretch of an interfacial H_2O molecule is $|\phi_d\rangle \propto \frac{\gamma}{\delta}|b\rangle + |d\rangle$, where $|b\rangle$ and $|d\rangle$ indicate vibrations localized, respectively, on uncoupled bOH and dOH groups, γ is the coupling between dOH and bOH stretch modes, and δ is the frequency difference between the uncoupled modes. Second-order perturbation theory yields $\frac{\gamma_{dOH}}{\delta_{dOH}} \sim 0.24$.[45] Taking the decay of the coupled dOH to be through the bOH portion of the wave function, we expect an intrinsic population lifetime (i.e., a lifetime in the absence of jumps from dOH to bOH) of $k^{d}_{IET} \sim (0.24)^2 k^{b}_{IVR}$. Estimating k^{b}_{IVR} from the lifetime of the bOH of HDO in bulk D_2O, for which $k^{b}_{IVR} \approx (0.75 \pm 0.05\ \text{ps})^{-1}$,[44] we obtain $k^{d}_{IET} \sim (13\ \text{ps})^{-1}$.

6. COMPARISON OF DANGLING OH DYNAMICS AT AIR/WATER AND HYDROPHOBIC/WATER INTERFACES

Experimentally, we find the jump time for an interfacial dOH group to form a HB at the ODS/water interface is 1.61 ± 0.10 ps. This is significantly slower than the 1.1 ps result previously reported[9,10] for the air/water interface. This result is surprising since the hydrophobic/water and air/water interfaces have commonly been considered to be similar.[48] We now use MD simulations to understand this difference in the interfacial water dynamics.

For the vapor/liquid interface and the hydrophobic/liquid interface, dOH groups are defined using the instantaneous

DOI: 10.1021/jacs.6b01820
J. Am. Chem. Soc. 2016, 138, 5551−5560

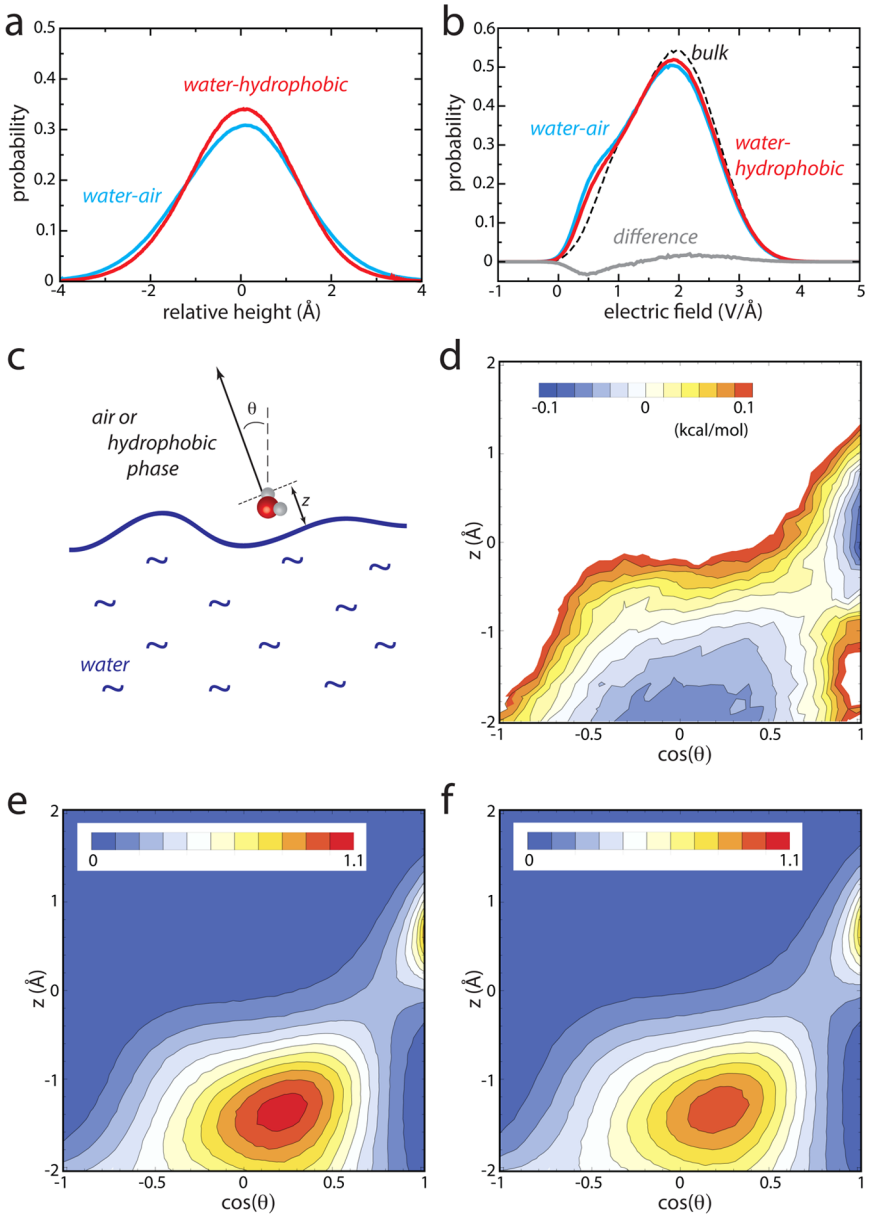

Figure 6. Structural features of the aqueous interfaces. (a) Distribution of the relative height of the instantaneous interface in each point of the grid with respect to the average surface height (=Gibbs surface) (blue, air/water; red, hexane/water). The interfacial widths are very similar. (b) Distributions of the electric field experienced by hydrogen atoms of tangent OHs, projected onto the OH axis, together with the difference between the hydrophobic and air interfacial distributions. As compared to the bulk, the distributions at the interface take slightly lower values and exhibit a shoulder at very low field values. (c) Definitions of the distance to the instantaneous interface and of the orientation of an OH group. (d) Two-dimensional free energy difference distribution $\Delta F(z,\cos\theta)$. (e, f) Two-dimensional probability distributions of the OH group distance to the interface (z) and orientation with respect to the surface normal vector ($\cos\theta$) at the hydrophobic and air interfaces, respectively.

interface, which provides an explicit description of capillary waves (Figure 5a, b). The jump time-correlation function[18] to go from a dOH to a bOH state is calculated as the probability for an OH group that is initially in a dangling configuration to be in a hydrogen-bonded configuration after a delay t,

$$C_j(t) = 1 - \langle p_d(0)p_b(t)\rangle \tag{11}$$

where $p_{d(b)}(t)$ is the probability to be in a dOH (bOH) state at time t. The results shown in Figure 5c for the two interfaces confirm that the simulations reproduce the faster dangling dynamics at the air/water interface relative to the hydrophobic/water interface. For the determination of jump times, we follow the same approach as that used to analyze the experiments (see above), and we consider the dynamics only after the initial decay ($t > T = 0.6$ ps). The jump times are then calculated by time-integration of the jump time-correlation function, $\tau_j = \int_T^\infty dt\, C_j(t)/C_j(T)$. This leads to dOH jump times of 1.7 ps at the hydrophobic interface and of 1.4 ps at the air interface. The results are in quantitative agreement with the measurements of the ODS/water interface and are qualitatively consistent with the report of $k^F_{jump} = (1.1\text{ ps})^{-1}$ at the air/water interface,[10] though the absence of reported uncertainty in the latter case and differences in data analysis prohibit a precise assessment of the degree of quantitative agreement. In addition, while the jump dynamics determined from simulations may depend on details of the dangling definition, we note that the trend

DOI: 10.1021/jacs.6b01820
J. Am. Chem. Soc. 2016, 138, 5551−5560

between the two types of interfaces seems to be robust. Indeed our present results agree with the values obtained in prior studies using the same water model respectively at an oil/water interface[49] ($\simeq$ 1.7 ps by reanalyzing the data of ref 49 with the same jump time definition as here) and at the air/water interface (0.8 ps[19]). The latter time is faster than the present value, most probably because the dangling groups are defined with respect to the Gibbs interface and so include transient HB breaks from the bulk. We note that the outermost dOH groups (i.e., those least likely to include transient HB breaks in the bulk) in Figure 12 of ref 19 reveal a forward jump time of approximately 1.3 ps.

We now investigate the molecular origin of the slower dynamics at the hydrophobic/liquid interface, as compared to the air/liquid interface. We first compare the structures of the two interfaces. Figure 6a shows that the interfacial widths are very similar in both cases, in agreement with prior simulations at the interface between water and air, and between water and a model hydrophobic liquid.[48,50] The protrusion of the hydrophobic groups in the water phase that had been suggested in ref 51 is thus not supported by our nor prior simulations.[52]

We next consider the strength of the hydrogen bonds at the two interfaces. Because it is not hydrogen-bonded, a dOH initially reorients quickly within a large cone[14] and the formation of a new HB may thus be less limited by the motion of this dOH than by the availability of a HB acceptor in its vicinity. The formation of a new HB is not diffusion-limited in contrast to a recent suggestion,[19] and it may depend on the HB exchange dynamics of OH groups that are tangent to the interface. The jump model showed that the free energy barrier that determines the HB jump dynamics arises both from the free energy cost to elongate the initial HB and from that for the approach of the new partner.[32,53−55] To jump from a bOH tangent state to a dOH configuration, no new partner is necessary and excluded-volume considerations[53] on the latter's approach do not apply (we note that a recent discussion[49] of the limitations of the excluded-volume picture for interfaces may need to be revised since the calculation of the volume inaccessible to water depends on the finite size of the water molecules, which was neglected in this work).

We measured the HB strength for OH groups tangent to the interface via the electric field experienced by the water H atom. A small electric field corresponds to a weak HB.[33] Our results clearly show that for the two interfaces, interfacial tangent OH groups tend to form weaker hydrogen bonds than do bulk OH groups (Figure 6b) This weakening of hydrogen bonds at the air/water interface relative to the bulk is consistent with prior surface spectroscopy experiments[45] and with the distortion of these hydrogen bonds reported in simulations.[52] However, the electric field distributions for both interfaces are largely similar, and only a very small increase in weak-field, i.e., weak HB, configurations can be found at the air/water interface relative to the hydrophobic/water interface, in agreement with the conclusions of recent SFG measurements.[51]

Since the difference in interfacial dangling dynamics does not arise from a difference in bOH HB strengths, we examine the stability of the dOH states. We consider the two-dimensional probability distribution $p(z,\cos\theta)$ for OH groups to be found with their hydrogen atom at a distance z from the instantaneous interface, and with an angle θ with respect to the normal to the interface (see Figure 6c). These distributions shown in Figure 6e and f for the two interfaces clearly reveal the stable dangling and tangent arrangements, in agreement with prior work on the air/water interface.[56] However, the free energy difference between the two interfaces for each location, defined as $\Delta F(z,\cos\theta) = -k_B T \ln[p_{\text{hydrophobic}}(z,\cos\theta)/p_{\text{air}}(z,\cos\theta)]$, reveals that the dangling configuration is stabilized by $\Delta F_d \simeq -0.1$ kcal/mol at the hydrophobic interface relative to the air interface, while the free energy of the transition state geometry between the dangling and tangent configurations is almost unchanged (see Figure 6d). This causes a slowdown of the dangling jump dynamics of approximately $\exp(\Delta F_d/k_B T) \simeq 1.2$, in agreement with our jump times computed directly from the jump time-correlation functions ($1.7/1.4 \approx 1.2$). Our simulations thus suggest that the slower dynamics at the hydrophobic interface is due to a greater stabilization of the dangling configuration, probably due to weak electrostatic interactions between the water OH groups and the hydrocarbon chains (we note that in the SPC/E water model employed here, the hydrogen atoms do not carry any van der Waals interaction center).

7. CONCLUSION

In conclusion, high-sensitivity measurements of the orientational dynamics of water at an interface with a hydrophobic self-assembled monolayer reveal the out-of-plane orientational motion of the dangling OH to occur on a time scale of 1.61 $\pm$ 0.10 ps, twice as fast as the orientational motion of water in bulk and about 50% slower than the out-of-plane orientational motion at the air/water interface.[10] Our MD simulations reproduce and confirm this trend and find a jump time of 1.7 ps at the hydrophobic-liquid/water interface.

Our simulations further show that the hydrophobic-water and air/water interfaces possess very similar structures, in agreement with previous studies.[48] However, we find that the dangling OH configurations are slightly more stabilized at the hydrophobic interface, which quantitatively explains the slower dangling dynamics as compared to the air/water interface. These observations extend our understanding of the unique properties of hydrophobic aqueous interfaces beyond what can be gleaned from static spectroscopy and may offer insights into the role of fluctuations of the hydrogen-bond network in biological and chemical processes involving hydrophobic interactions.

AUTHOR INFORMATION

Corresponding Authors

*damien.laage@ens.fr

*mcguire@pa.msu.edu

Notes

The authors declare no competing financial interest.

ACKNOWLEDGMENTS

The authors acknowledge support from the National Science Foundation (Grant No. CHE-1151590).

REFERENCES

(1) Levy, Y.; Onuchic, J. N. *Annu. Rev. Biophys. Biomol. Struct.* **2006**, *35*, 389.

(2) Frauenfelder, H.; Chen, G.; Berendzen, J.; Fenimore, P. W.; Jansson, H.; McMahon, B. H.; Stroe, I. R.; Swenson, J.; Young, R. D. *Proc. Natl. Acad. Sci. U. S. A.* **2009**, *106*, 5129.

(3) Narayan, S.; Muldoon, J.; Finn, M. G.; Fokin, V. V.; Kolb, H. C.; Sharpless, K. B. *Angew. Chem., Int. Ed.* **2005**, *44*, 3275.

(4) Jung, Y. S.; Marcus, R. A. *J. Am. Chem. Soc.* **2007**, *129*, 5492.

DOI: 10.1021/jacs.6b01820
J. Am. Chem. Soc. 2016, 138, 5551−5560

(5) Limmer, D. T.; Willard, A. P.; Madden, P.; Chandler, D. *Proc. Natl. Acad. Sci. U. S. A.* **2013**, *110*, 4200.
(6) McGuire, J. A.; Shen, Y. R. *Science* **2006**, *313*, 1945.
(7) Smits, M.; Ghosh, A.; Sterrer, M.; Muller, M.; Bonn, M. *Phys. Rev. Lett.* **2007**, *98*, 098302.
(8) Eftekhari-Bafrooei, A.; Borguet, E. *J. Phys. Chem. Lett.* **2011**, *2*, 1353.
(9) Hsieh, C. S.; Campen, R. K.; Verde, A. C. V.; Bolhuis, P.; Nienhuys, H. K.; Bonn, M. *Phys. Rev. Lett.* **2011**, *107*, 116102.
(10) Hsieh, C. S.; Campen, R. K.; Okuno, M.; Backus, E. H. G.; Nagata, Y.; Bonn, M. *Proc. Natl. Acad. Sci. U. S. A.* **2013**, *110*, 18780.
(11) Nienhuys, H. K.; Bonn, M. *J. Phys. Chem. B* **2009**, *113*, 7564.
(12) Gengeliczki, Z.; Rosenfeld, D. E.; Fayer, M. D. *J. Chem. Phys.* **2010**, *132*, 244703.
(13) Lee, S. H.; Rossky, P. J. *J. Chem. Phys.* **1994**, *100*, 3334.
(14) Stirnemann, G.; Rossky, P. J.; Hynes, J. T.; Laage, D. *Faraday Discuss.* **2010**, *146*, 263.
(15) Fecko, C. J.; Loparo, J. J.; Roberts, S. T.; Tokmakoff, A. *J. Chem. Phys.* **2005**, *122*, 054506.
(16) Rezus, Y. L. A.; Bakker, H. J. *J. Chem. Phys.* **2005**, *123*, 114502.
(17) Laage, D.; Hynes, J. T. *Science* **2006**, *311*, 832.
(18) Laage, D.; Hynes, J. T. *J. Phys. Chem. B* **2008**, *112*, 14230.
(19) Vila Verde, A.; Bolhuis, P. G.; Campen, R. K. *J. Phys. Chem. B* **2012**, *116*, 9467.
(20) Eaves, J. D.; Loparo, J. J.; Fecko, C. J.; Roberts, S. T.; Tokmakoff, A.; Geissler, P. L. *Proc. Natl. Acad. Sci. U. S. A.* **2005**, *102*, 13019.
(21) Eftekhari-Bafrooei, A.; Borguet, E. *J. Am. Chem. Soc.* **2010**, *132*, 3756.
(22) Shen, Y. R. *J. Phys. Chem. C* **2012**, *116*, 15505.
(23) Harris, A. L.; Rothberg, L. *J. Chem. Phys.* **1991**, *94*, 2449.
(24) Abragam, A. *The Principles of Nuclear Magnetism*; Clarendon Press: Oxford, 1961.
(25) Murphy, W. F. *Mol. Phys.* **1978**, *36*, 727.
(26) Sagiv, J. *J. Am. Chem. Soc.* **1980**, *102*, 92.
(27) Ghosh, A.; Smits, M.; Bredenbeck, J.; Dijkhuizen, N.; Bonn, M. *Rev. Sci. Instrum.* **2008**, *79*, 093907.
(28) Willard, A. P.; Chandler, D. *J. Phys. Chem. B* **2010**, *114*, 1954.
(29) Phillips, J. C.; Braun, R.; Wang, W.; Gumbart, J.; Tajkhorshid, E.; Villa, E.; Chipot, C.; Skeel, R. D.; Kale, L.; Schulten, K. *J. Comput. Chem.* **2005**, *26*, 1781.
(30) Berendsen, H. J. C.; Grigera, J. R.; Straatsma, T. P. *J. Phys. Chem.* **1987**, *91*, 6269.
(31) Feller, S. E.; MacKerell, A. D. *J. Phys. Chem. B* **2000**, *104*, 7510.
(32) Laage, D.; Stirnemann, G.; Sterpone, F.; Rey, R.; Hynes, J. T. *Annu. Rev. Phys. Chem.* **2011**, *62*, 395.
(33) Gruenbaum, S. M.; Tainter, C. J.; Shi, L.; Ni, Y.; Skinner, J. L. *J. Chem. Theory Comput.* **2013**, *9*, 3109.
(34) Stirnemann, G.; Wernersson, E.; Jungwirth, P.; Laage, D. *J. Am. Chem. Soc.* **2013**, *135*, 11824.
(35) Du, Q.; Freysz, E.; Shen, Y. R. *Science* **1994**, *264*, 826.
(36) Tian, C. S.; Shen, Y. R. *Proc. Natl. Acad. Sci. U. S. A.* **2009**, *106*, 15148.
(37) Lock, A. J.; Bakker, H. J. *J. Chem. Phys.* **2002**, *117*, 1708.
(38) Ye, S.; Nihonyanagi, S.; Uosaki, K. *Phys. Chem. Chem. Phys.* **2001**, *3*, 3463.
(39) Eftekhari-Bafrooei, A.; Nihonyanagi, S.; Borguet, E. *J. Phys. Chem. C* **2012**, *116*, 21734.
(40) Zhang, Z.; Piatkowski, L.; Bakker, H. J.; Bonn, M. *Nat. Chem.* **2011**, *3*, 888.
(41) Ashihara, S.; Huse, N.; Espagne, A.; Nibbering, E. T. J.; Elsaesser, T. *Chem. Phys. Lett.* **2006**, *424*, 66.
(42) Woutersen, S.; Bakker, H. J. *Nature* **1999**, *402*, 507.
(43) Cowan, M. L.; Bruner, B. D.; Huse, N.; Dwyer, J. R.; Chugh, B.; Nibbering, E. T. J.; Elsaesser, T.; Miller, R. J. D. *Nature* **2005**, *434*, 199.
(44) Woutersen, S.; Emmerichs, U.; Nienhuys, H. K.; Bakker, H. J. *Phys. Rev. Lett.* **1998**, *81*, 1106.
(45) Stiopkin, I. V.; Weeraman, C.; Pieniazek, P. A.; Shalhout, F. Y.; Skinner, J. L.; Benderskii, A. V. *Nature* **2011**, *474*, 192.
(46) Corcelli, S. A.; Skinner, J. L. *J. Phys. Chem. A* **2005**, *109*, 6154.
(47) Loparo, J. J.; Roberts, S. T.; Nicodemus, R. A.; Tokmakoff, A. *Chem. Phys.* **2007**, *341*, 218.
(48) Willard, A. P.; Chandler, D. *J. Chem. Phys.* **2014**, *141*, 18c519.
(49) Chen, M.; Lu, X. C.; Liu, X. D.; Hou, Q. F.; Zhu, Y. Y.; Zhou, H. Q. *J. Phys. Chem. C* **2015**, *119*, 16639.
(50) Bresme, F.; Chacon, E.; Tarazona, P.; Tay, K. *Phys. Rev. Lett.* **2008**, *101*, 056102.
(51) Strazdaite, S.; Versluis, J.; Backus, E. H. G.; Bakker, H. J. *J. Chem. Phys.* **2014**, *140*, 054711.
(52) Jedlovszky, P. *J. Phys.: Condens. Matter* **2004**, *16*, S5389.
(53) Laage, D.; Stirnemann, G.; Hynes, J. T. *J. Phys. Chem. B* **2009**, *113*, 2428.
(54) Sterpone, F.; Stirnemann, G.; Hynes, J. T.; Laage, D. *J. Phys. Chem. B* **2010**, *114*, 2083.
(55) Stirnemann, G.; Laage, D. *J. Phys. Chem. Lett.* **2010**, *1*, 1511.
(56) Liu, J.; Andino, R. S.; Miller, C. M.; Chen, X.; Wilkins, D. M.; Ceriotti, M.; Manolopoulos, D. E. *J. Phys. Chem. C* **2013**, *117*, 2944.

DOI: 10.1021/jacs.6b01820
J. Am. Chem. Soc. 2016, 138, 5551−5560